An Enzymatically Cleavable Tripeptide Linker for Maximizing the Therapeutic Index of Antibody–Drug Conjugates

Summer Y.Y. Ha[1], Yasuaki Anami[1], Chisato M. Yamazaki[1], Wei Xiong[1], Candice M. Haase[2], Scott D. Olson[2], Jangsoon Lee[3], Naoto T. Ueno[3], Ningyan Zhang[1], Zhiqiang An[1], and Kyoji Tsuchikama[1]

ABSTRACT

Valine–citrulline is a protease-cleavable linker commonly used in many drug delivery systems, including antibody–drug conjugates (ADC) for cancer therapy. However, its suboptimal *in vivo* stability can cause various adverse effects such as neutropenia and hepatotoxicity, leading to dose delays or treatment discontinuation. Here, we report that glutamic acid–glycine–citrulline (EGCit) linkers have the potential to solve this clinical issue without compromising the ability of traceless drug release and ADC therapeutic efficacy. We demonstrate that our EGCit ADC resists neutrophil protease–mediated degradation and spares differentiating human neutrophils. Notably, our anti-HER2 ADC shows almost no sign of blood and liver toxicity in healthy mice at 80 mg kg^{-1}. In contrast, at the same dose level, the FDA-approved anti-HER2 ADCs Kadcyla and Enhertu show increased levels of serum alanine aminotransferase and aspartate aminotransferase and morphologic changes in liver tissues. Our EGCit conjugates also exert greater antitumor efficacy in multiple xenograft tumor models compared with Kadcyla and Enhertu. This linker technology could substantially broaden the therapeutic windows of ADCs and other drug delivery agents, providing clinical options with improved efficacy and safety.

Introduction

Targeted drug delivery has attracted increasing attention as a means to improve drug efficacy while reducing toxicity to healthy tissues. In particular, antibody–drug conjugates (ADC), mAbs linked with pharmacologically active molecules (payloads) via chemical linkers, are one of the most promising classes with remarkable and durable treatment effects; they have been used for the treatment of cancers (1, 2) and other diseases (3, 4). The clinical success of this drug class has been demonstrated with 12 FDA-approved ADCs for a broad range of hematologic malignancies and solid tumors (5) and more than 100 candidates in clinical trials (clinicaltrials.gov). Despite recent advances in ADC chemistry, medical oncology, and clinical management, ADC-based treatment often entails various side effects, including myelosuppression and liver toxicity. Thus, ADC technologies capable of minimizing the risk of adverse effects can be used to implement effective cancer therapy without impairing patient quality of life.

The ADC linker is a critical component that influences the overall drug efficacy and safety profiles (6, 7). Cleavable linkers are used for nearly 70% of ADCs to efficiently liberate conjugated payloads inside the target cancer cells, leading to increased ADC potency (8). Among them, cathepsin-sensitive valine–citrulline (VCit) and similar dipeptide linkers connecting a payload via a *p*-aminobenzyloxycarbonyl (PABC) spacer are most commonly used as an industry-standard technology. Indeed, this linker system is used in more than 40 ADCs (9), such as Adcetris (10), Polivy (11), Padcev (12), Zynlonta (13), and Tivdak (**Fig. 1A**; ref. 14). However, patients treated with VCit-based ADCs and similar conjugates often suffer from dose-limiting toxicities. In phase II and III studies of Adcetris, an ADC equipped with monomethyl auristatin E (MMAE) through VCit linkers, neutropenia (16%–22% of patients; refs. 15–17) and hepatotoxicity (7% of patients; ref. 17) were common side effects leading to dose delays or treatment discontinuation. In a phase I study of the anti-CD71 probody–VCit MMAE conjugate CX2029, grade 3 or higher neutropenia was observed in 33% of patients (18). Suboptimal linker stability may partly contribute to such toxicities. We have demonstrated that glutamic acid–valine–citrulline (EVCit) tripeptide is an enzymatically cleavable linker with improved plasma stability (**Fig. 1B**; ref. 19). The additional glutamic acid at the P_3 position markedly reduces susceptibility to extracellular carboxylesterase 1c (Ces1c) found in rodent plasma (20), preventing premature payload release from the linker in mouse circulation. Although advantageous preclinically, as is the case with VCit linkers (21), the EVCit linker was shown to be susceptible to human neutrophil elastase-mediated degradation (described in detail in the Results section). Consequently, the population of neutrophils can be suppressed by prematurely released payloads, which may eventually cause neutropenia in patients.

Here we show that glutamic acid–glycine–citrulline (EGCit) tripeptide linkers have the potential to solve the abovementioned clinical issues without compromising ADC therapeutic efficacy (**Fig. 1C**). The EGCit sequence provides long-term stability in both mouse and primate plasma, spares differentiating human neutrophils, and retains the capacity to quickly liberate free payloads upon intracellular cleavage. This study also suggests that MMAE ADCs constructed with EGCit linkers can exhibit improved antitumor activity in a panel of cancer cell lines and in three different xenograft mouse models when

[1]Texas Therapeutics Institute, The Brown Foundation Institute of Molecular Medicine, McGovern Medical School, The University of Texas Health Science Center at Houston, Houston, Texas. [2]Department of Pediatric Surgery, McGovern Medical School, The University of Texas Health Science Center at Houston, Houston, Texas. [3]Section of Translational Breast Cancer Research, Department of Breast Medical Oncology, The University of Texas MD Anderson Cancer Center, Houston, Texas.

S.Y.Y. Ha and Y. Anami contributed equally to the article.

Corresponding Author: Kyoji Tsuchikama, The Brown Foundation Institute of Molecular Medicine, The University of Texas Health Science Center at Houston, 1881 East Road, Houston, TX 77054. E-mail: kyoji.tsuchikama@uth.tmc.edu

Mol Cancer Ther 2022;21:1449–61

doi: 10.1158/1535-7163.MCT-22-0362

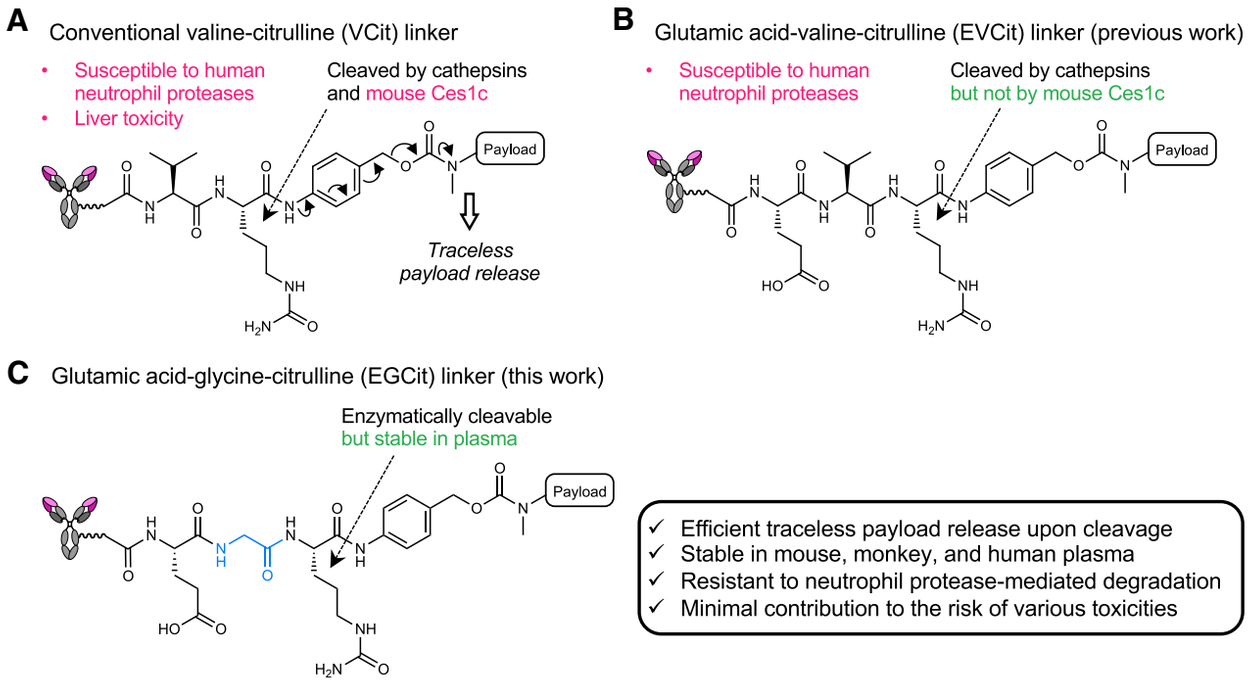

Figure 1.

The structures and stability profiles of cleavable peptide linkers. **A,** VCit-based ADC linker. VCit linkers are unstable in mouse circulation due to susceptibility to the extracellular Ces1c. VCit linkers are also labile to human neutrophil elastase–mediated degradation. This instability often triggers premature payload release, leading to poor efficacy in preclinical rodent models and safety concerns, including neutropenia and liver toxicity in humans. **B,** EVCit-based ADC linker. We have previously developed EVCit linkers that are stable in human and mouse plasma. However, as shown in this study, this linker is also incapable of withstanding neutrophil elastase–mediated degradation. **C,** EGCit-based ADC linker. This study demonstrates that EGCit linkers resist degradation in circulation and cleavage mediated by human neutrophil proteases while remaining capable of releasing payloads in a traceless manner upon intracellular cleavage.

compared with conventional conjugates, including FDA-approved anti-HER2 ADCs Kadcyla (T-DM1) and Enhertu (DS-8201). Notably, our EGCit-based ADC shows no significant myelosuppression or hepatotoxicity in healthy mice at 80 mg kg^{-1}. Our findings indicate that the EGCit linker technology not only ensures smooth transition from preclinical research to clinical studies, but also provides a broadly applicable solution for substantially widening therapeutic windows of targeted drug delivery systems, including ADCs.

Materials and Methods

Supplementary appendix

A comprehensive and detailed description of all compounds, antibodies and conjugates, and methods used in this study is also provided in the Supplementary Data.

Cell culture

U87ΔEGFR-luc was generated by lentiviral transduction of U87ΔEGFR cells (a gift from Dr. Balveen Kaur, UTHealth) using Lentifect lentiviral particles encoding for firefly luciferase and a puromycin-resistant gene (GeneCopoeia, LP461-025). Transduction was performed according to the manufacturer's instruction. This cell line is available from the authors for academic use upon reasonable request. JIMT-1 (AddexBio, RRID:CVCL_2077), SK-BR-3 (ATCC, RRID:CVCL_0033), and BT-474 (ATCC, RRID:CVCL_0179) were cultured in RPMI1640 (Corning) supplemented with 10% EquaFETAL (Atlas Biologicals), GlutaMAX (2 mmol/L, Gibco), sodium pyruvate (1 mmol/L, Corning), and penicillin-streptomycin (penicillin: 100 units mL^{-1}; streptomycin: 100 μg mL^{-1}, Gibco). KPL-4 (provided by Dr. Junichi Kurebayashi at Kawasaki Medical School, RRID:CVCL_5310), MDA-MB-453 (ATCC, RRID:CVCL_0418), MDA-MB-231 (ATCC, RRID:CVCL_0062), and U87ΔEGFR-luc were cultured in DMEM (Corning) supplemented with 10% EquaFETAL, GlutaMAX (2 mmol/L), and penicillin-streptomycin (penicillin: 100 units mL^{-1}; streptomycin: 100 μg mL^{-1}). All cells were cultured at 37°C under 5% CO_2 and routinely tested using a Mycoalert *Mycoplasma* Contamination Kit (Lonza) to make sure there was no contamination in cell cultures. Cells were passaged before becoming fully confluent up to 20 passages. All cell lines were obtained from vendors or collaborators as described above within the period of 2014 to 2018, characterized by DNA profiling, and no further authentication was conducted by the authors. All cell lines were validated for antigen expression in cell-based ELISA prior to use.

Cell viability assay

Cells were seeded in a culture-treated 96-well clear plate (5,000 cells per well in 50 μL culture medium) and incubated at 37°C under 5% CO_2 for 24 hours. Serially diluted samples (50 μL) were added to each well and the plate was incubated at 37 °C for 72 hours for KPL-4, SK-BR-3, MDA-MB-231, and U87ΔEGFR-luc cells, and 96 hours for JIMT-1, BT-474, and MDA-MB-453 cells. For duocarmycin DM (DuoDM) ADCs, all the tested cell lines were incubated for 120 hours. After the old medium was replaced with 100 μL fresh medium, 20 μL of a mixture of WST-8 (1.5 mg mL^{-1}, Cayman chemical) and 1-methoxy-5-methylphenazinium methylsulfate (100 μmol/L, Cayman Chemical) was added to each well, and the plate was incubated at 37°C for 2 hours.

After gently agitating the plate, the absorbance at 460 nm was recorded using a BioTek Synergy HTX plate reader. EC_{50} values were calculated using Graph Pad Prism 9 software. All assays were performed in triplicate.

Human neutrophil killing assay

CD34-positive hematopoietic stem and progenitor cells (HSPC) isolated from the bone marrow were differentiated into neutrophils following the protocol reported by Zhao and colleagues (21) with modifications (see Supplementary Data for details). On day 7 after differentiation, cell culture medium was replaced with fresh StemSpan SFEM II supplemented with GCSF (30 ng mL^{-1}), 1% penicillin-streptomycin, and vehicle control or each ADC (200 nmol/L) and cell density was adjusted to 1×10^5 cells mL^{-1}. After being incubated for 7 days (day 14), cells were measured for CD15 and CD66b by flow cytometry (see Supplementary Data for details). Effect of each ADC on the population of neutrophils was represented by percentage of CD66b/CD15 double-positive cells in the viable cell population relative to that of the untreated group.

Animal studies

All procedures were approved by the Animal Welfare Committee of the University of Texas Health Science Center at Houston and performed in accordance with the institutional guidelines for animal care and use. All animals were housed under controlled conditions, namely, 21°C–22°C (±0.5°C), 30%–75% (±10%) relative humidity, and 12:12 light/dark cycle with lights on at 7.00 am. Food and water were available *ad libitum* for all animals.

Tolerability study

Female CD-1 IGS mice (6–8 weeks old, Charles River Laboratories, Strain Code: 022) received a single dose of each ADC (80 mg kg^{-1}) intraperitoneally (vehicle, $n = 8$; Kadcyla, $n = 7$; Enhertu, $n = 7$; EGCit ADC **4c**, $n = 8$; MC-VCit MMAE drug-to-antibody ratio (DAR) 4 ADC, $n = 6$). Body weight was monitored every day for 5 days (Note: 4 mice in the vehicle group were used for the following blood chemistry analysis without body weight monitoring, thus these mice were not included in this tolerability assessment). Humane endpoints were defined as (i) greater than 20% weight loss or (ii) severe signs of distress. However, no mice met these criteria over the course of study. Five days after injection, these mice were deeply anesthetized with isoflurane and the whole blood was drawn by heart puncture for following blood chemistry and hematology analysis. For following histology analysis, livers were also harvested, fixed with 4% paraformaldehyde in cold PBS at 4°C for 2 days, immersed in cold PBS at 4°C for 24 hours, and stored in 70% ethanol until use.

Blood chemistry, histology, and hematology analysis

[1] Blood chemistry. Whole blood (400–600 μL) was drawn from a part of the mice used or prepared in the tolerability study described above (vehicle, $n = 4$; all other groups, $n = 3$) using S-Monovette charged with serum gel (1.1 mL syringe, Sarstedt) and allowed to clot at room temperature for 30–40 minutes. After centrifugation at 2,000 × *g* for 10 minutes, resulting serum samples (150 μL) were loaded onto NSAID 6 clips specialized for identifying liver damage (IDEXX) and analyzed using a Catalyst Dx Chemistry Analyzer (IDEXX). [2] Histology. Paraffin-embedded liver sections were prepared using the fixed livers and then stained using hematoxylin and eosin (H&E). Subsequently, bright-field images of the H&E-stained tissues (×20) were taken using a Nikon Eclipse Ti microscope. Images were processed using NIS-Element software (version 4.51.00) and analyzed using Image J. [3] Hematology. Whole blood (700–1,000 μL) was drawn from a part of the mice used in the tolerability study described above ($n = 4$ for all groups) using S-Monovette charged with ethylenediaminetetraacetic acid tripotassium salt (K_3 EDTA; 1.1 mL syringe, Sarstedt). Blood samples were gently mixed well by inversion and stored on ice until analysis (for less than 4 hours). Each blood sample (500 μL) was analyzed using a Procyte Dx (IDEXX).

In vivo xenograft mouse models of human breast cancer

[1] KPL-4 model. Cells (1×10^7 cells) suspended in 100 μL of 1:1 PBS/Cultrex BME Type 3 (Trevigen) were orthotopically injected into the inguinal mammary fat pad of female NOD *scid* gamma (NSG) mice (6–8 weeks old, purchased from The Jackson Laboratory, stock number: 005557, maintained by in-house breeding). When the tumor volume reached approximately 100 mm^3, mice were randomly assigned to six groups ($n = 5$ for each group) and a single dose of each ADC (1 mg kg^{-1}) or vehicle was administered to mice intravenously. Tumor volume ($0.52 \times a \times b^2$, *a*: long diameter, *b*: short diameter) and body weight were monitored twice a week using a digital caliper and a digital balance. Mice were euthanized when the tumor volume exceeded 1,000 mm^3, the tumor size exceeded 2 cm in diameter, greater than 20% weight loss was observed, or mice showed signs of distress. Such events were counted as deaths. [2] JIMT-1/MDA-MB-231 admixed tumor model. A cosuspension of 1×10^7 JIMT-1 cells and 2.5×10^6 MDA-MB-231 cells in 100 μL of 1:1 PBS/Cultrex BME Type 3 (Trevigen) was orthotopically injected into the inguinal mammary fat pad of female NU/J mice (6–8 weeks old, The Jackson Laboratory, stock number: 002019). On day 7 after transplantation, mice were randomly assigned to each group ($n = 5$ for Enhertu; $n = 6$ for EGCit-MMAE/F dual-drug ADC **7a**) and injected intravenously with sterile-filtered human IgG (30 mg kg^{-1}, Innovative Research, catalog number: IRHUGGFLY1G) in PBS. The next day, a single dose of Enhertu (3 mg kg^{-1}) or dual-drug ADC **7a** (1 mg kg^{-1}) was administered to mice intravenously. Tumor volume ($0.52 \times a \times b^2$, *a*: long diameter, *b*: short diameter) and body weight were monitored twice a week. Mice were euthanized when the tumor volume exceeded 1,000 mm^3, the tumor size exceeded 2 cm in diameter, or mice showed severe signs of distress. Such events were counted as deaths.

Orthotopic xenograft mouse model of human glioblastoma

U87ΔEGFR-luc cells (1×10^5 cells) were stereotactically implanted into NSG mice (6–8 weeks old, male) as follows. NSG mice were injected intraperitoneally with a cocktail of ketamine (67.5 mg kg^{-1}) and dexmedetomidine (0.45 mg kg^{-1}) and maintained at 37°C on a heating pad until the completion of surgery. After the head skin was shaved and treated with 10 μL of 0.25% bupivacaine supplemented with epinephrine (1:200,000), anesthetized mice were placed on a stereotactic instrument. After disinfecting the head skin with chlorhexidine and ethanol, a small incision was made and then a burr hose was drilled into the skull over the right hemisphere (1 mm anterior and 2 mm lateral to the bregma). A 10 μL Hamilton syringe (model 701 N) was loaded with cells suspended in 2 μL cold Hank's Balanced Salt Solution and slowly inserted into the right hemisphere through the burr hole (3.5 mm depth). After a 1-minute hold time, cells were injected over a 5-minute period (0.4 μL min^{-1}). After a 3-minute hold time, the needle was retracted at a rate of 0.75 mm $minute^{-1}$. The incision was closed using GLUture (Zoetis) and mice were injected with atipamezole (1 mg kg^{-1}, i.p.). At day 5 after implantation, brain tumor-bearing NSG mice were randomized and injected intravenously with a single dose of either ADC (5 mg kg^{-1}, $n = 6$ for VCit ADC **8a**; $n = 7$ for EGCit ADC **8b**) or PBS ($n = 6$). Body weight was monitored

every 3–4 days and mice were euthanized when body weight loss of >20% or any severe clinical symptom was observed. Such events were counted as deaths.

Statistical analysis

Although no statistical analysis was performed prior to performing experiments, sample size was determined by following methods for similar experiments in the field reported previously. We did not use the vehicle control in the xenograft breast cancer studies for statistical analysis. The investigators were not blinded to allocation during experiments. For the quantification of intracellularly released MMAE and human neutrophil viability assay, a one-way ANOVA with a Dunnett *post hoc* test was used for multiple comparisons. For blood chemistry and hematology analysis and xenograft tumor model studies, a Welch *t* test (two-tailed, unpaired, uneven variance) was used. Kaplan–Meier survival curve statistics were analyzed with a logrank (Mantel–Cox) test. To control the familywise error rate in multiple comparisons, crude *P* values were adjusted by the Holm–Bonferroni method. Differences with $P_{adjusted}$ values less than 0.05 were considered statistically significant in all analysis. See Supplementary Table S9 for all *P* values.

Data availability

All data supporting the findings in this study are available within the article, its Supplementary Data, or from the corresponding author upon reasonable request.

Results

Incorporating glycine at the P_2 position and glutamic acid at the P_3 position increases resistance to undesired degradation leading to premature payload release

To seek alternatives to the conventional VCit linker with improved *in vivo* stability and tolerability, we first investigated how the linker instability leading to neutropenia could be circumvented. Serine proteases secreted extracellularly from differentiating human neutrophils have been shown to promote the release of MMAE from VCit-based ADCs, reducing the population of bone marrow neutrophils (21). With this in mind, we set out to identify the cleavage site by neutrophil elastase using small-molecule probes (see Supplementary Data for synthesis details). VCit–PABC–pyrene probe **1** was incubated with human neutrophil elastase at 37°C for 24 hours. A pyrene fragment containing citrulline–PABC was found to be the major product by liquid chromatography–electrospray ionization-mass spectrometry (ESI-MS; **Fig. 2A**). This result indicates that neutrophil elastase cleaves the amide bond between P_1 citrulline and P_2 valine. Although no supporting data were presented, Miller and colleagues recently reported the same observation (22). EVCit probe **2** also yielded the same citrulline-containing fragment, suggesting that glutamic acid at P_3 does not protect the linker from neutrophil elastase–mediated degradation.

On the basis of this initial analysis, we screened various amino acids at the P_2 position. We prepared a panel of pyrene probes containing an EXCit–PABC unit where X is glycine (**3a**), alanine (**3b**), leucine (**3c**), and isoleucine (**3d**; **Fig. 2B**). We also prepared EV(*N*-Me)Cit probe **3e** and GCit dipeptide probe **3f** (see Supplementary Data for synthesis details). Subsequently, all probes were tested for stability against human neutrophil elastase–mediated degradation (**Fig. 2C**). Surprisingly, EVCit probe **2** degraded more quickly than VCit probe **1**, indicating that the P_3 glutamic acid can increase the linker susceptibility to elastase-mediated degradation. EACit and EICit probes **3b**,**d** also rapidly degraded. These results are consistent with a previous study demonstrating that human neutrophil elastase preferentially cleaves the *N*-terminus amide bonds of valine, alanine, and isoleucine (23). In contrast, we observed marginal or almost no degradation for probes containing EGCit (**3a**), ELCit (**3c**), EV(*N*-Me)Cit (**3e**), or GCit (**3f**). This observation suggests that the P_2 amino acid impacts the reactivity with neutrophil elastase more significantly than the P_3 amino acid. We further tested EGCit and EV(*N*-Me)Cit probes **3a**,**e** for resistance to cleavage by other abundant proteases secreted by human neutrophils: human proteinase 3 and cathepsin G. EGCit probe **3a** was completely intact in the presence of either protease while EV(*N*-Me)Cit probe **3e** was partially degraded by proteinase 3 (Supplementary Table S1).

Next, we tested probes **3a**–**f** for stability in undiluted BALB/c mouse plasma (**Fig. 2D**). EGCit, EACit, and EV(*N*-Me)Cit probes **3a**,**b**,**e** showed improved stability compared with EVCit probe **2**. In particular, about 45% of EGCit probe **3a** remained intact after a 4-day incubation. GCit probe **3f** was less stable than EGCit probe **3a**, which is consistent with our previous finding that glutamic acid at the P_3 position enhances linker stability in mouse plasma. Furthermore, EGCit probe **3a** completely withstood degradation in monkey and human plasma (**Fig. 2E**; Supplementary Table S2). Finally, we performed another set of stability assays for EFCit, E(*N*-Me)VCit, (*N*-Me)VCit, and V(*N*-Me)Cit probes. However, these probes exhibited promoted degradation in mouse plasma or cleavage mediated by neutrophil elastase (Supplementary Fig. S1). Collectively, these findings suggest that the EGCit sequence offers greatly enhanced stability against undesired proteolytic degradation leading to premature payload release.

EGCit linker increases ADC hydrophilicity and cell killing potency with efficient intracellular payload release

We set out to investigate how the P_2 amino acids evaluated above affect ADC physicochemical properties, intracellular payload release upon cleavage, and antigen-specific cell killing potency. To this end, we constructed anti-HER2 ADCs using selected P_2-modified cleavable linkers and the conjugation technology developed by our group (**Fig. 3A**; refs. 19, 24, 25). First, diazide branched linkers were site-specifically installed onto the side chain of glutamine 295 (Q295) within N297A anti-HER2 mAb (derived from trastuzumab) by microbial transglutaminase (MTGase)-mediated transpeptidation. In parallel, we prepared EVCit, EGCit, EV(*N*-Me)Cit, and GCit linker-based modules containing bicyclo[6.1.0]nonyne (BCN) as a handle for strain-promoted azide–alkyne cycloaddition, polyethylene glycol, PABC as a self-immolative spacer, and MMAE as a payload (see Supplementary Data for synthesis details). Finally, these payload modules underwent the click reaction with the mAb–tetraazide to afford homogeneous anti-HER2 ADCs **4a**–**e** with a DAR of 4. The homogeneity of each conjugate was confirmed by ESI-MS analysis (**Fig. 3B**; Supplementary Data). We confirmed by size-exclusion chromatography (SEC) analysis that no significant dissociation or aggregation occurred after incubating each ADC in PBS (pH 7.4) at 37°C for 28 days (Supplementary Fig. S2). Subsequently, we performed hydrophobic interaction chromatography (HIC) analysis under physiologic conditions (phosphate buffer, pH 7.4) to assess the relative hydrophobicity of each ADC (**Fig. 2C**). EGCit ADC **4c** was the least hydrophobic of the ADCs tested. EVCit ADC **4b**, EV(*N*-Me)Cit ADC **4d**, and GCit ADC **4e** had intermediate hydrophobicity. VCit ADC **4a** was the most hydrophobic conjugate. This result suggests that incorporating the smallest amino acid glycine at the P_2 position and negatively charged glutamic acid at the P_3 position can synergistically

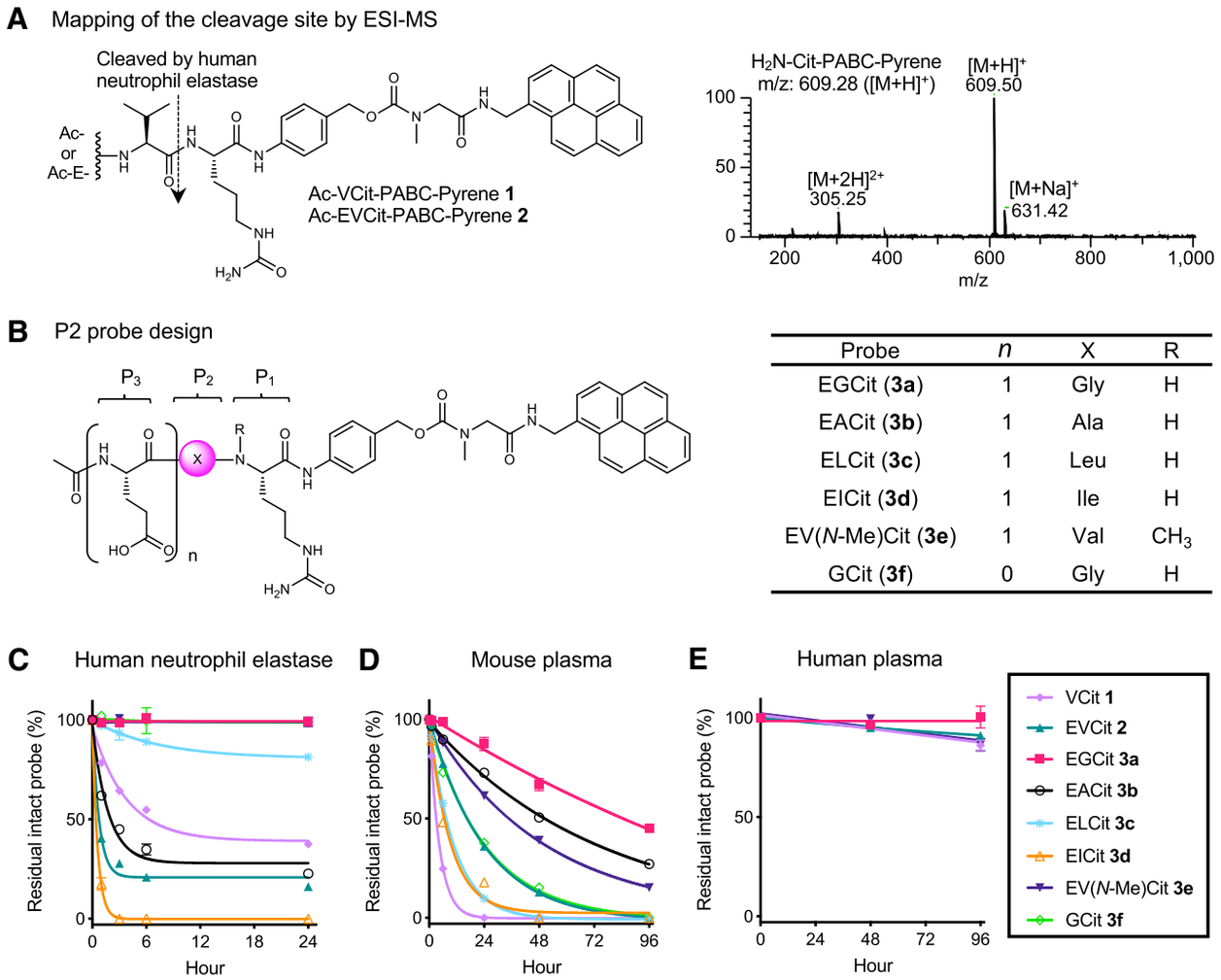

Probe	*n*	X	R
EGCit (**3a**)	1	Gly	H
EACit (**3b**)	1	Ala	H
ELCit (**3c**)	1	Leu	H
EICit (**3d**)	1	Ile	H
EV(*N*-Me)Cit (**3e**)	1	Val	CH_3
GCit (**3f**)	0	Gly	H

Figure 2.

Incorporating glycine at the P_2 position and glutamic acid at the P_3 position increases resistance to undesired degradation leading to premature payload release. **A,** ESI-MS–based mapping of the cleavage site in the presence of human neutrophil elastase. We observed cleavage of the amide bond between valine and citrulline within VCit (**1**) and EVCit (**2**) probes. **B,** Structures of small-molecule P_2 probes containing EGCit (**3a**), EACit (**3b**), ELCit (**3c**), EICit (**3d**), EV(*N*-Me)Cit (**3e**), or GCit (**3f**). A pyrene group was used as a surrogate of hydrophobic ADC payloads. **C–E,** Stability of probes **1**, **2**, and **3a–f** in the presence of human neutrophil elastase (**C**), in undiluted BALB/c mouse plasma (**D**), and in undiluted human plasma (**E**) at 37°C. (**1**) Light purple diamond; (**2**) green triangle; (**3a**) magenta square; (**3b**) black open circle; (**3c**) cyan asterisk; (**3d**) orange open triangle; (**3e**) purple inversed triangle; (**3f**) light green open diamond. All assays were performed at least three times in technical duplicate, and representative data from the replicates are shown ($n = 2$). Data are presented as mean values ±SEM. PABC, *p*-aminobenzyloxycarbonyl.

reduce ADC hydrophobicity at physiologic pH. This feature is advantageous in the construction of ADCs because hydrophobic ADCs often show high aggregation rates leading to fast clearance (26).

Next, we tested the ADCs for HER2-binding affinity using cell-based ELISA. We used the human breast cancer cell lines KPL-4 (HER2-positive) and MDA-MB-231(HER2-negative; Supplementary Fig. S2; Supplementary Table S3). We confirmed that all anti-HER2 ADCs retained high binding affinity for KPL-4 (K_D: 0.084–0.156 nmol/L) but not for MDA-MB-231. We then evaluated these ADCs for *in vitro* cytotoxicity in HER2-positive (KPL-4, SK-BR-3, BT-474, JIMT-1, MDA-MB-453) and HER2-negative (MDA-MB-231) human breast cancer cell lines (**Fig. 3D–I**). As controls, we also prepared and tested noncleavable anti-HER2 MMAE ADC **4f** (DAR 4) and an isotype control ADC constructed using the BCN–EGCit–PABC–MMAE module (**5**, DAR 4). VCit ADC **4a**, EVCit ADC **4b**, and EGCit ADC **4c** exhibited comparable cell killing potency in the HER2-positive cell lines, but not in HER2-negative MDA-MB-231 cells; under our assay conditions, the EC_{50} values of these ADCs were 0.070–0.084 nmol/L in KPL-4, 0.120–0.167 nmol/L in SK-BR-3, 0.470–0.543 nmol/L in BT-474, 0.086–0.110 nmol/L in JIMT-1, and 0.193–0.272 nmol/L in MDA-MB-453 (Supplementary Table S4). These ADCs also showed similar maximum cell killing potency at high concentrations (Supplementary Table S5). EV(*N*-Me)Cit ADC **4d** exhibited a similar EC_{50} value in SK-BR-3. However, its EC_{50} values and cell viability at high concentrations were greater than those of EGCit ADC **4c** in the other HER2-positive cell lines. GCit ADC **4e** was as potent as EGCit **4c** in KPL-4, JIMT-1, and BT-474; however, GCit ADC **4e** was less effective in SK-BR-3 and MDA-MB-453 than EGCit **4c** as indicated by the increased EC_{50} value and percentage of viable cells at the maximum ADC concentration. Noncleavable anti-HER2 ADC **4f**, which lacked a

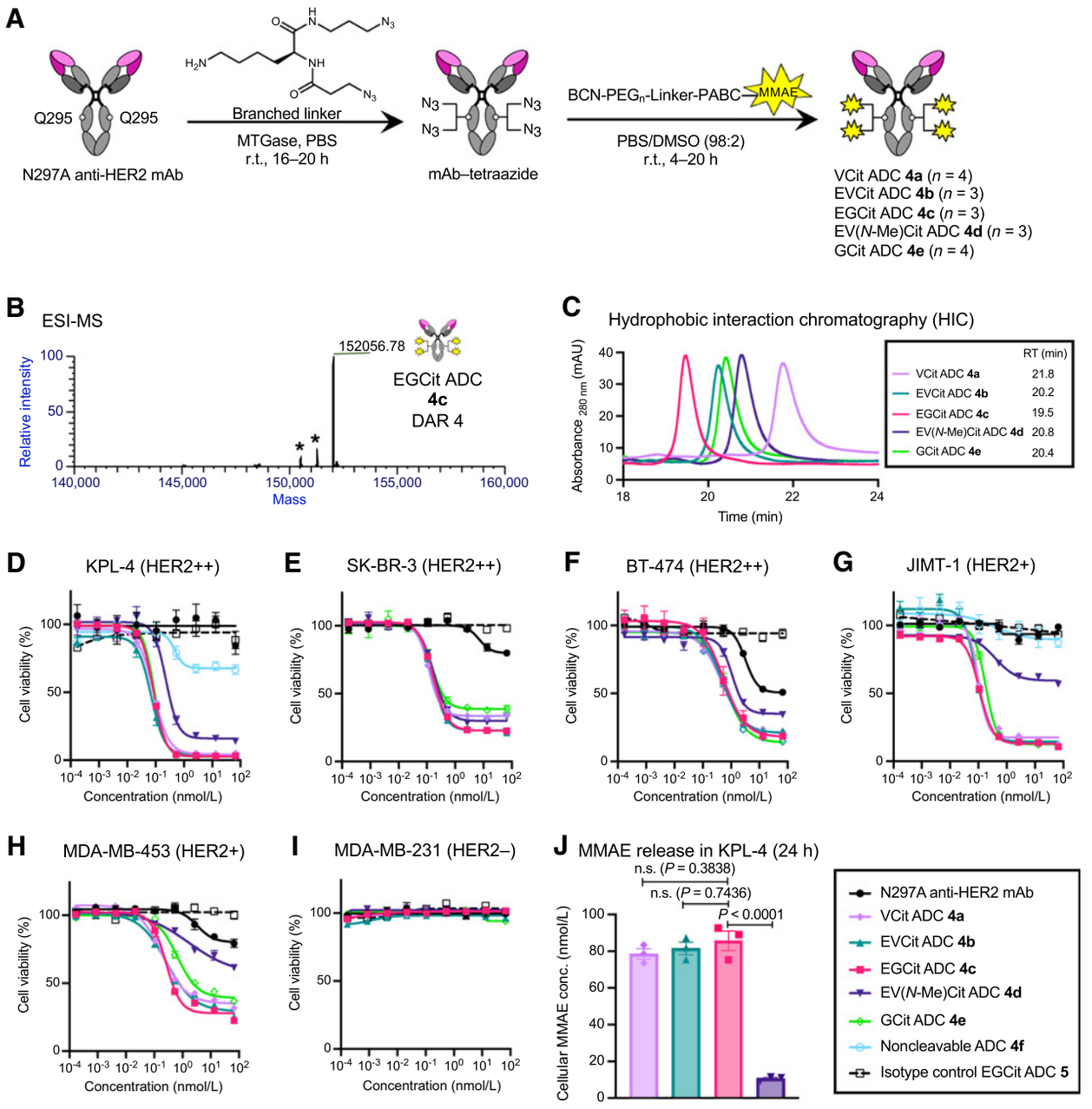

Figure 3.

EGCit linker increases ADC hydrophilicity and cell killing potency with efficient intracellular payload release. **A,** Construction of ADCs (**4a**–**e**) by MTGase-mediated branched linker conjugation and following strain-promoted azide–alkyne cycloaddition (yellow spark: MMAE). **B,** Deconvoluted ESI-MS trace of EGCit ADC **4c**. Asterisk (*) indicates a fragment ion detected in ESI-MS analysis. See Supplementary Data for mass traces of the other ADCs. **C,** Overlay of five HIC traces (VCit ADC **4a**: light purple; EVCit ADC **4b**: green; EGCit ADC **4c**: magenta; EV(*N*-Me)Cit ADC **4d**: purple; GCit ADC **4e**: light green) under physiologic conditions (phosphate buffer, pH 7.4). Cell killing potency in the breast cancer cell lines KPL-4 (**D**), SK-BR-3 (**E**), BT-474 (**F**), JIMT-1 (**G**), MDA-MB-453 (**H**), and MDA-MB-231 (**I**). We tested unconjugated N297A anti-HER2 mAb (black circle), VCit ADC **4a** (light purple diamond), EVCit ADC **4b** (green triangle), EGCit ADC **4c** (magenta square), EV(*N*-Me)Cit **4d** (purple inversed triangle), GCit ADC **4e** (light green open diamond), noncleavable ADC **4f** (cyan open circle), and isotype control EGCit ADC **5** (black open rectangle with dotted curve). **J,** ESI-MS–based quantification of free MMAE released from ADCs **4a**–**c** in KPL-4 cells after incubation at 37°C for 24 hours. All assays were performed in triplicate. Data are presented as mean values ± SEM. For statistical analysis, a one-way ANOVA with a Dunnett *post hoc* test was used (comparison control: EGCit ADC **4c**). BCN, bicyclo[6.1.0]nonyne; DAR, drug-to-antibody ratio; MMAE, monomethyl auristatin E; MTGase, microbial transglutaminase; n.s., not significant; PEG, polyethylene glycol; RT, retention time.

cleavable peptide sequence within the linker scaffold, showed far greater EC_{50} values in KPL-4 and JIMT-1 cells compared with cleavable ADCs **4a–c**. Furthermore, isotype control EGCit ADC **5** showed almost no cell killing effect in either cell line. These findings highlight the importance of internalization and the following intracellular release of free MMAE for effective cell killing. The comparable binding affinities and potencies also suggest that ADCs **4a–c** can deliver a similar amount of MMAE to the targeted cells. To verify this point, we quantified free MMAE released from ADC **4a–d** in KPL-4 cells (**Fig. 3J**). After treating KPL-4 cells with each ADC for 24 hours, the MMAE concentrations in cell lysates were determined by high-resolution ESI-MS. As anticipated, about 80% of conjugated MMAE was detected as a free payload in the groups of VCit, EVCit, and EGCit ADCs **4a–c**. In contrast, we observed only 10% MMAE release for EV(*N*-Me)Cit ADC **4d**, indicating that the *N*-methylation of the citrulline retarded the payload release. Detailed analysis of other parameters (e.g., internalization rate) in addition to linker cleavage will provide how each parameter influences the overall payload release kinetics and intracellular accumulation. Taken together, these results demonstrate that the hydrophilic EGCit sequence enables efficient traceless payload release upon ADC internalization in a wide range of cell types with varying catabolic profiles, ensuring maximal ADC potency.

EGCit ADC is stable in plasma and spares differentiating human neutrophils

To assess ADC stability and safety profiles, we first tested ADCs **4a–c** for plasma stability. We observed no significant degradation in either ADC after a 28-day incubation in undiluted human and monkey plasma at 37°C (**Fig. 4A** and **B**; Supplementary Tables S6 and S7). EVCit and EGCit ADCs **4b**,**c** showed almost no linker cleavage after a 14-day incubation in undiluted BALB/c mouse plasma (**Fig. 4C**; Supplementary Table S8). In contrast, VCit ADC **4a** lost approximately 74% of the conjugated MMAE after the same period of time. Next, we evaluated the stability of these ADCs in the presence of human neutrophil elastase (**Fig. 4D**). EVCit ADCs **4b** underwent partial degradation and DAR 0–3 fragments were generated. However, EGCit ADC **4c** completely resisted degradation. These results are consistent with the earlier studies using pyrene probes (**Fig. 2C–E**).

To investigate the potential effect of our ADCs on neutrophil production in human bone marrow, we performed *ex vivo* differentiation of HSPCs into neutrophils followed by ADC treatment (**Fig. 4E**). Zhao and colleagues reported that the population of differentiating human neutrophils was markedly decreased by ADCs equipped with MMAE via a VCit linker, but mature neutrophils could tolerate the toxic effect (21). Following their protocol with some modifications, we differentiated HSPCs collected from a single donor into granulocytes with growth factors over a period of 7 days. At this point, the population of viable cells expressing both granulocyte markers CD15 and CD66b increased from 0.7% to 71.3% (**Fig. 4F** and **G**; Supplementary Fig. S3). Because neutrophils are the most abundant granulocyte type in humans (50%–75% of all leukocytes), we considered these CD15/CD66b double-positive cells to be a population representing differentiating neutrophils. Then, these cells were treated with 200 nmol/L of EVCit and EGCit ADCs **4b**,**c**. For EGCit ADC **4c**, we did not observe a significant decrease in the percentage of $CD15^+$/$CD66b^+$ cells relative to that in the vehicle group (**Fig. 4H**; Supplementary Fig. S3). In contrast, the relative neutrophil population significantly decreased to 55% by treatment with EVCit ADC **4b**. Collectively, these results highlight the potential of the EGCit linker to reduce the risk of myelosuppression, in particular neutropenia caused by prematurely released ADC payloads.

EGCit linker has the potential to minimize the antigen-independent myelotoxicity and hepatotoxicity of ADCs

To investigate whether or not the cleavable EGCit linker alters ADC safety at therapeutic doses, we performed an exploratory toxicology study. Healthy CD-1 IGS mice were injected with EGCit MMAE ADC **4c**, Enhertu, or Kadcyla at 80 mg kg^{-1} and monitored over the course of 5 days. A maleimide-linked VCit MMAE ADC was also tested as a conventional example. We did not observe any significant body weight loss or other severe clinical symptom in the treatment groups, except in the maleimide–VCit ADC group; all mice treated with this ADC lost about 15% of their body mass, and one mouse died on day 3 (Supplementary Fig. S4). Next, to evaluate the potential liver toxicity of our ADC and the two approved ADCs, a blood chemistry test was performed by collecting serum at the end of the 5-day monitoring (**Fig. 5A–D**). We quantified the following molecules associated with liver functions: alanine aminotransferase (ALT), aspartate aminotransferase (AST), alkaline phosphatase (ALKP), and blood urea nitrogen (BUN). Increased ALT, AST, and ALKP as well as decreased BUN generally indicate liver damage. In the case of our EGCit ADC, the values of these parameters were comparable with those of the untreated cohort. In contrast, mice treated with Enhertu and Kadcyla showed elevated ALT, elevated AST, and decreased BUN. The ALKP level also appeared to increase with these two ADCs. We validated this observation by performing histologic analysis using livers collected from the mice (**Fig. 5E–H**). We observed a marginal amount of nucleus condensation for most of the tissue samples collected from the EGCit ADC group (**Fig. 5F**). Compared with this group, condensed nuclei and inflamed regions were more evident in tissue samples treated with Enhertu and Kadcyla (**Fig. 5G** and **H**). In addition, we observed hepatocellular ballooning and nucleus fragmentation in the Kadcyla group (**Fig. 5H**). These findings indicate that both EGCit ADC **4c** and Enhertu caused low to moderate hepatocyte apoptosis and that Kadcyla caused severe liver damage. Hematologic analysis was also performed by collecting whole blood on day 5. We observed no significant change in red blood cell, platelet, and neutrophil counts for our ADC or Enhertu compared with the untreated cohort. In contrast, 3 of 4 mice treated with Kadcyla showed markedly decreased platelet counts and increased neutrophil counts (Supplementary Fig. S4), which is consistent with previous observations (27–29). Although more detailed pathologic analysis needs to be performed, we observed significant decreases in platelet (2 of 3 mice) and neutrophil counts (1 of 3 mice) for VCit ADC **S21**. This observation demonstrates that the VCit ADC was much less tolerated than the other ADCs tested probably because of its instability in mouse circulation, precluding precise assessment of toxicity profiles. Overall, these results suggest that the safety of our EGCit MMAE ADC is greater than that of its clinical competitors.

EGCit ADCs exert improved antitumor effects in various xenograft models compared with conventional ADCs

We sought to evaluate EGCit-based ADCs for treatment efficacy in multiple xenograft mouse tumor models (**Fig. 6A–F**). In the KPL-4 inflammatory breast tumor model, orthotopically xenografted NSG mice were injected intravenously with a single dose of our anti-HER2 ADCs **4b**,**c**, Kadcyla, or Enhertu at 1 mg kg^{-1}. To examine the applicability of our EGCit linker technology, we also prepared and tested DuoDM ADCs **6** (see Supplementary Notes). This ADC showed subnanomolar EC_{50} values in vitro (0.114 nmol/L in KPL-4 and 0.060 nmol/L in JIMT-1) as seen for MMAE ADC **4c**, demonstrating that the EGCit linker can also release DuoDM efficiently (Supplementary Fig. S5; Supplementary Table S3). We did not observe any

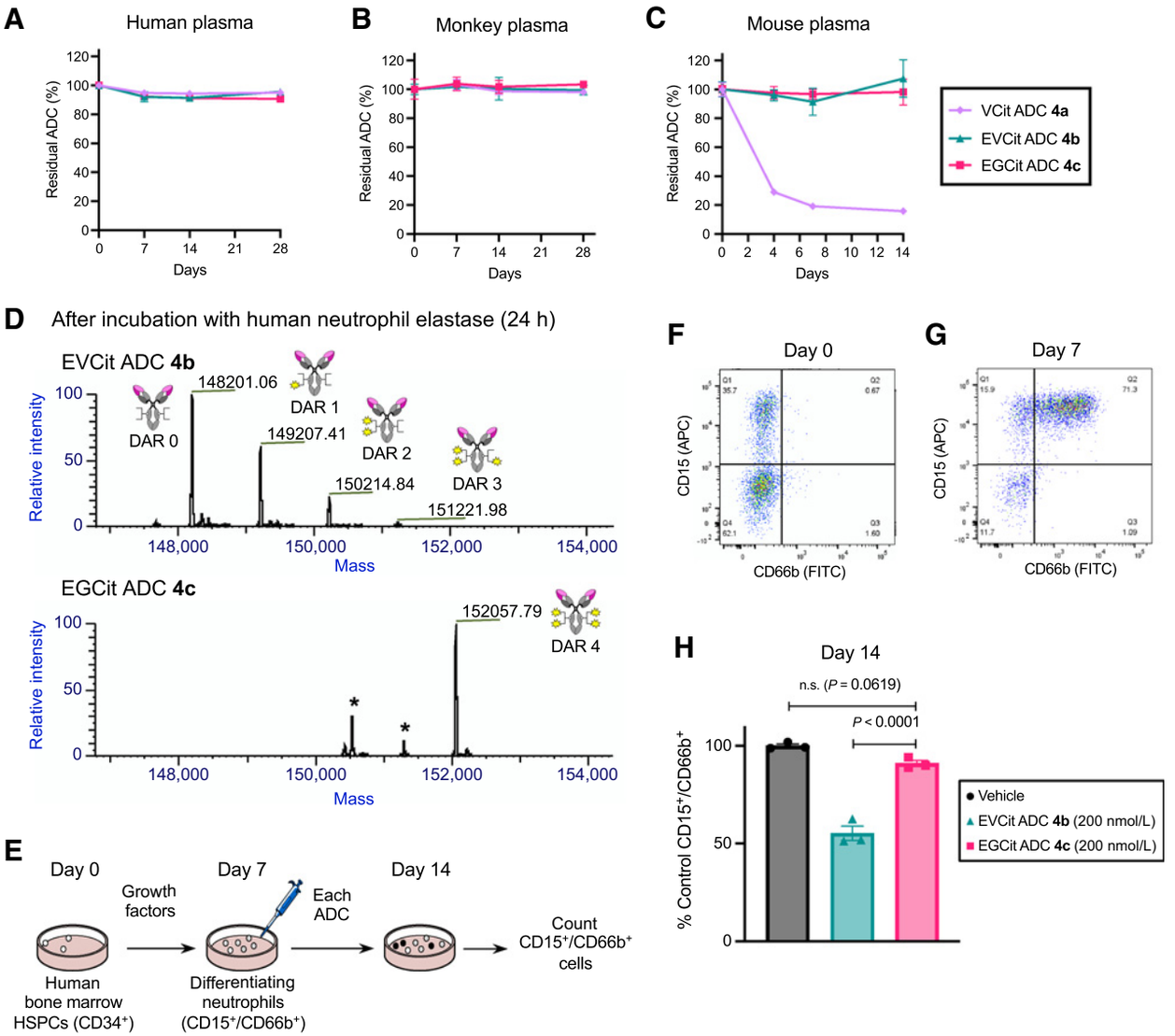

Figure 4.

EGCit ADC is stable in plasma and spares differentiating human neutrophils derived from the bone marrow. Stability at 37°C in undiluted human plasma (**A**), cynomolgus monkey plasma (**B**), and BALB/c mouse plasma (**C**). VCit ADC **4a** (light purple diamond), EVCit ADC **4b** (green triangle), and EGCit ADC **4c** (magenta square) were tested. **D,** ESI-MS traces of ADCs **4b**,**c** after incubation with human neutrophil elastase at 37°C for 24 hours. EGCit ADC **4c** did not undergo cleavage, whereas EVCit ADC **4b** underwent linker degradation and lost part of its payloads. **E,** Study schedule for differentiation of human bone marrow HSPCs into neutrophils and subsequent treatment with ADCs **4b**,**c**. After 3-day expansion (day 0), HSPCs were treated with growth factors for 7 days and differentiated into $CD15^+$ and $CD66b^+$ granulocytes/neutrophils. **F** and **G,** Flow cytometry before (day 0; **F**) and after (day 7; **G**) differentiation. **H,** The effects of ADCs (vehicle, dark gray; EVCit ADC **4b**, green; EGCit ADC **4c**, magenta) on the population of human neutrophils relative to those of vehicle control ($n = 3$). All assays were performed in triplicate. Data are presented as mean values ±SEM. For statistical analysis, a one-way ANOVA with a Dunnett *post hoc* test was used (comparison control: EGCit ADC **4c**). HSPC, hematopoietic stem and progenitor cell.

significant acute toxicity associated with administration of ADCs **4b**,**c** and **6** over the course of study as evaluated by monitoring significant body weight loss and other clinical symptoms (Supplementary Fig. S6). In addition, these ADCs exhibited remarkable percent tumor growth inhibition (%TGI on day 31: 107%, ADC **4b**; 104%, ADC **4c**; 94%, ADC **6**) and survival benefits (animal death by day 70: no death, **4b**,**c**; 1 of 5 mice, ADC **6**; **Fig. 6A** and **B**; Supplementary Fig. S6). In contrast, compared with EGCit ADC **4c**, only limited tumor growth inhibition was observed for Kadcyla (47%TGI, $P = 0.0097$) and Enhertu (48%TGI, $P = 0.0158$). All animals treated with these FDA-approved ADCs were found dead or killed at the predefined humane endpoint (>1,000 mm^3 tumor size or >20% body weight loss) by the end of the study (median survival time: 35 days, Kadcyla, 45 days, Enhertu).

Next, we tested the clinical potential of the EGCit linker in the dual-drug ADC format. We have demonstrated that a dual-drug ADC equipped with MMAE and MMAF can effectively treat HER2-low heterogeneous breast tumors with elevated drug resistance (30). We

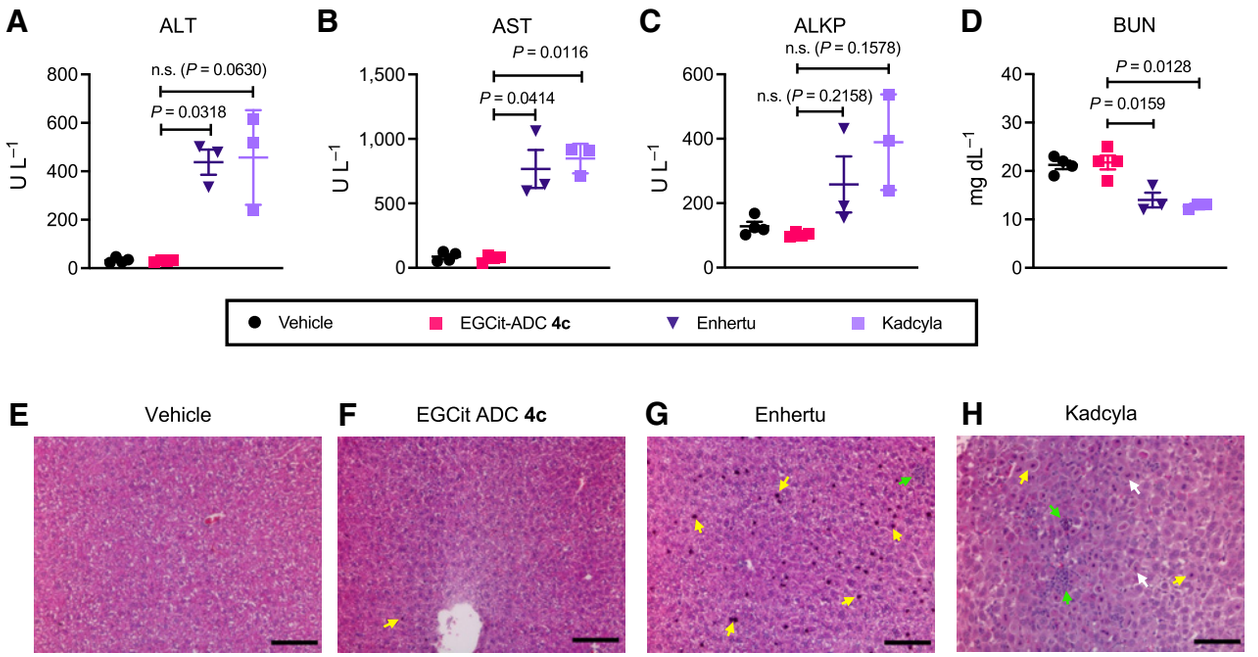

Figure 5.

The EGCit linker has the potential to minimize antigen-independent hepatotoxicity of ADCs. Blood chemistry parameters [ALT (**A**), AST (**B**), ALKP (**C**), and BUN (**D**)] measured 5 days after ADC injection to 6–8 weeks female CD-1 mice. Mice were injected intravenously with a single dose of vehicle control ($n = 4$), EGCit ADC **4c** (magenta square, $n = 4$), Enhertu (purple inversed triangle, $n = 3$), or Kadcyla (light purple square, $n = 3$) at 80 mg kg^{-1}. Data are presented as mean values (bars) ± SEM. For statistical analysis, a Welch *t* test (two-tailed, unpaired, uneven variance) was used. To control the familywise error rate in multiple comparisons, crude *P* values were adjusted by the Holm–Bonferroni method. H&E-stained liver sections 5 days after treatment with vehicle (**E**), EGCit ADC **4c** (**F**), Enhertu (**G**), or Kadcyla (**H**). Morphological changes are indicated with color arrows (yellow: condensed nuclei; green: necrosis and inflammation; white: fragmented nuclei). Scale bar, 100 μmol/L. This experiment was repeated more than twice independently with similar results. ALKP, alkaline phosphatase; ALT, alanine aminotransferase; AST, aspartate aminotransferase; BUN, blood urea nitrogen, H&E, hematoxylin and eosin.

prepared EGCit-based MMAE/F DAR 4+2 ADC **7a** (see Supplementary Data for details). This ADC and Enhertu were tested in the JIMT-1/MDA-MB-231 admixed tumor model established by our group previously: a model of refractory human breast cancer characterized by aggressive growth, heterogeneous low HER2 expression, and moderate resistance to hydrophobic payloads such as MMAE (30). A single dose of each ADC (Enhertu, 3 mg kg^{-1}; ADC **7a**, 1 mg kg^{-1}) was intravenously administered to orthotopic tumor-bearing nude mice 8 days after implantation (average tumor volume: 100–150 mm^3). No acute toxicity associated with ADC administration was observed for either ADC (Supplementary Fig. S6). EGCit dual-drug ADC **7a** exhibited remarkable antitumor effects (112%TGI on day 31; **Fig. 6C**; Supplementary Fig. S6) and survival benefits (no animal death by day 70; **Fig. 6D**). This treatment outcome is comparable with our observation for EVCit variant **7b** (107%TGI on day 31) tested in our previous study (30), suggesting that the cleavable EGCit linker is as good at enhancing *in vivo* ADC efficacy and circulation stability as our previous EVCit linker. In contrast, even with an increased dose (3 mg kg^{-1}), Enhertu exhibited only moderate inhibition of tumor growth in this HER2 heterogeneous tumor model (76%TGI on day 31, $P = 0.0065$, comparison control: EGCit ADC **7a**). Furthermore, 4 of 5 mice needed to be euthanized by the end of the study due to severe clinical symptoms, including tumor ulceration.

Although these studies indicate the superiority of our linker system, readers should be aware that the dosing schedule of each ADC was not adjusted on the basis of the differences in pharmacokinetics. The payload-based half-lives of Kadcyla and Enhertu at the elimination phase are 3–5 days (31) and 8.23 days (32), respectively. On the basis of the high structural similarity to our previous EVCit ADCs (19, 30), we expect the half-lives of EGCit ADCs are 12–16 days. As such, Kadcyla and Enhertu could have exhibited better efficacy in our studies with dose adjustment. Even so, the EGCit linker system is likely advantageous from a therapeutic window standpoint based on its improved safety profiles, as shown in **Fig. 5**.

Finally, we set out to establish the generalizability of our linker technology by testing in an orthotopic glioblastoma multiforme (GBM) model (**Fig. 6E** and **F**). ADC-based systemic treatment of GBM has been unsuccessful as demonstrated by the recent failure of depatuxizumab mafodotin (formerly called ABT-414; ref. 33) and AMG-595 (34) in clinical trials. Using our linker technology, we could construct a panel of homogeneous anti-EGFR variant III (EGFRvIII) ADCs from N297A depatuxizumab, including conventional VCit ADC **8a**, EGCit ADC **8b**, and EGCit–DuoDM ADCs conjugated via PABC or *p*-aminobenzyl quaternary ammonium (35) linkage (see Supplementary Data for preparation and characterization details). These ADCs were equally potent in EGFRvIII-positive U87ΔEGFR-luc GBM cells (Supplementary Fig. S5). ADCs **8a**,**b** were then tested in the orthotopic U87ΔEGFR-luc model (**Fig. 6E**). Intracranial tumor-bearing NSG mice were injected intravenously with a single dose of each ADC at 5 mg kg^{-1} 5 days post-implantation. No acute toxicity associated with ADC administration was observed in either group (Supplementary Fig. S6). The short survival time of the untreated cohort (median survival time: 16 days) demonstrates the aggressive

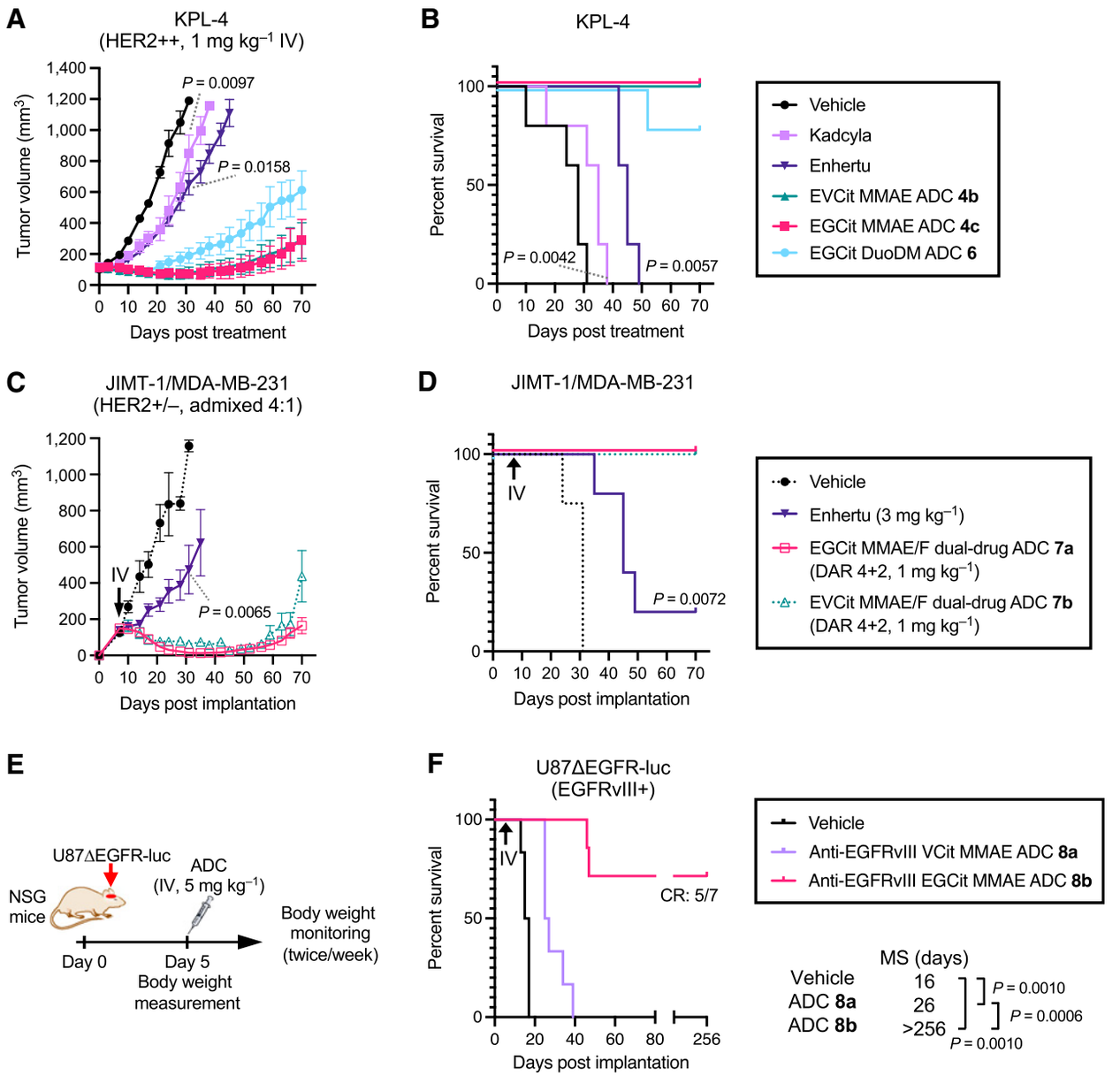

Figure 6.

EGCit ADCs exert improved antitumor effects in various xenograft models compared with conventional ADCs. Antitumor activity (**A**, **C**) and survival benefit (**B**, **D**) in orthotopic xenograft mouse models of human breast cancer. KPL-4 model (**A**, **B**): a single dose of vehicle control (black circle), Kadcyla (light purple square), Enhertu (purple inversed triangle), EVCit-MMAE ADC **4b** (green triangle), EGCit-MMAE ADC **4c** (magenta square), or EGCit-DuoDM ADC **6** (cyan circle) was intravenously administered at 1 mg kg^{-1} to tumor-bearing female NSG mice at a mean tumor volume of approximately 100 mm^3 ($n = 5$ for all groups). JIMT-1/MDA-MB-231 4:1 admixed model (**C**, **D**): 8 days after implantation (indicated with a black arrow), female NU/J mice were intravenously administered with a single dose of Enhertu (3 mg kg^{-1}, purple inversed triangle, $n = 5$) or EGCit-MMAE/F DAR 4+2 dual-drug ADC **7a** (1 mg kg^{-1}, magenta open square, $n = 6$). Note: The tumor volume and survival curve data of vehicle control (black circle with dotted curve, $n = 4$) and EVCit dual-drug ADC **7b** (1 mg kg^{-1}, green open triangle with dotted curve, $n = 5$) presented here were previously reported by our group (30). Data are presented as mean values ± SEM. Study schedule in the U87ΔEGFR-luc orthotopic xenograft model (**E**) and survival curves after treatment (**F**). U87ΔEGFR-luc cells were intracranially implanted to male NSG mice. Five days after implantation, mice were intravenously administered with a single dose of vehicle control (black, $n = 6$), anti-EGFRvIII VCit-MMAE ADC **8a** (5 mg kg^{-1}, light purple, $n = 6$), or anti-EGFRvIII EGCit-MMAE ADC **8b** (5 mg kg^{-1}, magenta, $n = 7$). All animals other than the ones that were found dead or achieved complete remission were killed at the predefined humane endpoint, which were counted as deaths. For statistical analysis of the tumor volume data, a Welch *t* test (two-tailed, unpaired, uneven variance) was used. Kaplan–Meier survival curve statistics were analyzed with a log-rank (Mantel–Cox) test. To control the familywise error rate in multiple comparisons, crude *P* values were adjusted by the Holm–Bonferroni method. CR, complete remission; DuoDM, duocarmycin DM.

tumor growth of this model (**Fig. 6F**). EGCit ADC **8b** exerted remarkable therapeutic efficacy; the median survival time was extended to >256 days, and 5 of 7 mice achieved complete remission without any symptoms or tumor lesions at the end of the study (confirmed by MRI 256 days after tumor implantation; Supplementary Fig. S6). In contrast, conventional VCit ADC **8a** moderately extended the median survival time to 26 days ($P = 0.001$, vs. vehicle; $P = 0.0006$, vs. EGCit ADC **8b**). All mice treated with VCit ADC **8a** died or were euthanized by the end of study.

Discussion

Cleavable linkers with excellent *in vivo* stability and broad applicability are the holy grail in the field of drug delivery. Although various ADC linkers have been developed to date, either ADC efficacy or safety profile has been suboptimal in many cases. The use of stable, noncleavable linkers (i.e., linkers without a defined cleavage mechanism) is a substantial option for avoiding premature linker cleavage. While some ADC payloads exhibit high potency irrespective of linker cleavage (e.g., MMAF; ref. 36), many payloads require conjugation via cleavable linkers to exert full potential (e.g., MMAE, duocarmycins, and pyrrolobenzodiazepine dimers; refs. 36–38). These studies suggest that any residual functional group resulting from linker cleavage can lower the potency of such payloads, highlighting the necessity of traceless payload release. Incorporating a defined linker cleavage site is also crucial to ensure that such payloads can effectively exert the bystander effect upon intracellular release. However, the use of ADCs with cleavable linkers such as VCit often entails an increased risk of adverse effects and low tolerability caused by undesired payload release prior to reaching cancer milieu (21, 36, 39). Indeed, previous studies have reported that most VCit MMAE-based ADCs and similar conjugates at 10–40 mg kg^{-1} show dose-limiting hepatotoxicity in rodents (40–42). Linkers developed recently [e.g., β-glucuronide–based linkers (26, 43)] may have the capacity to address this dilemma with their unique payload release mechanisms (22, 44). However, the applicability of those linkers to a broad range of cancer types has not yet been fully validated. For instance, the expression level of β-glucuronidase in tumor cells has been shown to vary substantially (45). As such, the payload release efficiency and therapeutic efficacy of β-glucuronide linker-based ADCs can be limited depending on the catabolic profiles of target tumors (26, 43).

This study demonstrates that the EGCit and structurally similar linkers (e.g., DGCit, EGQ, EGA) could potentially provide a general solution to circumvent clinical safety issues with their excellent *in vivo* stability against multiple degradation events, without losing the capability of traceless payload release. We have found that our previous EVCit linker is sensitive to human neutrophil protease–mediated degradation like conventional VCit linkers. We have identified that the P_2 valine within the VCit linker provokes degradation mediated by human neutrophil proteases. In addition, we have shown that replacing the valine with glycine effectively protects the linker from this degradation. Compared with VCit-based linkers, the EGCit linker also showed significantly decreased hydrophobicity and increased stability in mouse, monkey, and human plasma. In addition, our EGCit-based ADCs exhibited antigen-specific cytotoxicity comparable with that of conventional VCit and our previous EVCit variants in various cancer cell lines with different metabolic profiles. Along with the remarkable tumor suppression efficacy observed for various mAb–payload combinations in multiple refractory breast and brain tumor models, these findings demonstrate the broad applicability of our cleavable EGCit linker technology. Incorporating a hydrophobic amino acid such as valine at the P_2 position has been commonly thought to be important to enable rapid cathepsin B–mediated linker cleavage (46, 47). However, our results indicate that such linker design is not a prerequisite to enable traceless payload release rapidly enough to maximize overall *in vivo* efficacy. Indeed, we have confirmed that most MMAE molecules conjugated via EGCit linkers are released in KPL-4 cells in a traceless manner within 24 hours. Recent reports have also demonstrated that a structural or stereochemical alteration to the P_2 amino acid does not necessarily abrogate intracellular cleavage of similar ADC linkers due to the potential involvement of other cathepsins (37, 48). On the basis of these and our findings, we speculate that proteases other than cathepsin B also play a role in traceless payload release from the EGCit linker. Although not yet performed, in-depth mechanistic studies will clarify how the interplay of proteases contribute to intracellular cleavage of the unconventional EGCit sequence.

Attenuating antigen-independent toxicities is a challenge not only for VCit-based ADCs but also for other ADCs, regardless of linker type and cleavability. In addition to neutropenia and thrombocytopenia, hepatotoxicity is another common adverse effect that can lead to dose delays or discontinuation of treatment in severe cases. For example, 15%–24% of patients with HER2-positive breast cancer treated with Kadcyla (containing a noncleavable linker) and Enhertu (containing a cleavable tetrapeptide linker) showed increases in liver damage-associated enzymes, namely, ALT and AST (49, 50). As was the case with Mylotarg (an anti-CD33 maytansinoid ADC with a disulfide cleavable linker; ref. 51), XMT-1522/TAK-522 (an anti-HER2 ADC highly loaded with an auristatin analog via a labile ester linker; ref. 52), and MEDI4276 (an anti-HER2 biparatopic ADC equipped with tubulysin via a cleavable lysine linker; ref. 53), severe liver toxicity can be a reason for clinical hold, study discontinuation, or withdrawal from the market. The exploratory toxicology studies presented here suggest that our EGCit cleavable linker minimally contributes to the risk of neutropenia, thrombocytopenia, and hepatotoxicity; healthy mice tolerated a single bolus dose of our anti-HER2 EGCit MMAE ADC at 80 mg kg^{-1} without exhibiting significant changes in hematologic parameters or liver tissue integrity. On the basis of the concept of allometric scaling, this dose level in mice is deemed equivalent to 6.5 mg kg^{-1} in humans (calculated with a conversion factor of 12.3; ref. 54). Considering this, the tolerability of this ADC in humans may be higher than that of many ADCs currently available in the clinic (for instance, the MTD of Kadcyla in humans is 3.6 mg kg^{-1}). However, in-depth pharmacokinetics and toxicology studies in other models, in particular nonhuman primates (i.e., models expressing target antigens in normal tissues), remain to be performed for further validation. In addition, testing ADCs with the same payload/DAR and different linkers will help better understand the advantages of EGCit-based ADCs. Such efforts will also provide more clinically relevant toxicology data (including antigen-dependent toxicity) and insights into the risk of side effects, including ones that were not evaluated in this study (e.g., peripheral neuropathy; ref. 55).

In summary, our findings support the conclusion that the cleavable EGCit linker has the potential to substantially broaden ADC therapeutic window. Because of its structural simplicity, desirable physicochemical properties, and independence from conjugation modality and payload type, this linker technology may be preferred for a variety of ADCs and other targeted drug delivery systems. However, it is important to note that the linker is not the only component determining therapeutic window; target antigen, mAb structure, payload type, the degree of payload loading, and conjugation method can also impact ADC efficacy and toxicity profiles. In our case, both the aglycosylated parent mAbs and our homogeneous conjugation may

have played a role in minimizing overall toxicity by reducing uptake by immune cells and the liver. Therefore, any new ADC should be carefully designed by considering all these parameters. With comprehensive molecular design optimization, we believe that the EGCit linker technology will help expand the repertoire of effective, safe targeted drug delivery systems; this may provide clinicians and patients with cancer with access to otherwise unrealistic treatment options such as high-dose ADC therapy.

Authors' Disclosures

S.Y.Y. Ha reports a patent for relating to the work pending. Y. Anami reports grants from the Japan Society for the Promotion of Science during the conduct of the study; in addition, Y. Anami has a patent for PCT/US2018/034363 issued, a patent for US-2020-0115326-A1 issued, a patent for EU18804968.8-1109/3630189 issued, and a patent for relating to the work pending. C.M. Yamazaki reports a patent for PCT/US2018/034363 issued, a patent for US-2020-0115326-A1 issued, a patent for EU18804968.8-1109/3630189 issued, and a patent for relating to the work pending. S.D. Olson reports grants from NIH NCATS/AstraZeneca outside the submitted work. N. Zhang reports grants from Cancer Prevention and Research Institute of Texas during the conduct of the study; in addition, N. Zhang has a patent for PCT/US2018/034363 issued, a patent for US-2020-0115326-A1 issued, a patent for EU18804968.8-1109/3630189 issued, and a patent for a provisional patent pending. Z. An reports other support from UT System during the conduct of the study; grants from CPRIT, CPRIT, and Welch Foundation outside the submitted work; in addition, Z. An has a patent for UT System pending. K. Tsuchikama reports grants from the National Institute of General Medical Sciences, the Department of Defense, and the Cancer Prevention and Research Institute of Texas during the conduct of the study; in addition, K. Tsuchikama has a patent for PCT/US2018/034363 issued, a patent for US-2020-0115326-A1 issued, a patent for EU18804968.8-1109/3630189 issued, and a patent for relating to the work pending. No disclosures were reported by the other authors.

Authors' Contributions

S.Y.Y. Ha: Formal analysis, validation, investigation, visualization, methodology, writing–original draft, writing–review and editing. **Y. Anami:** Formal analysis, funding acquisition, validation, investigation, visualization, methodology, writing–original draft, writing–review and editing. **C.M. Yamazaki:** Formal analysis, investigation, visualization, methodology, writing–review and editing. **W. Xiong:** Validation, investigation, methodology. **C.M. Haase:** Formal analysis, validation, investigation, visualization, methodology. **S.D. Olson:** Formal analysis, methodology. **J. Lee:** Resources. **N.T. Ueno:** Resources. **N. Zhang:** Resources, methodology. **Z. An:** Resources, funding acquisition, methodology. **K. Tsuchikama:** Conceptualization, resources, supervision, funding acquisition, investigation, methodology, writing–original draft, project administration, writing–review and editing.

Acknowledgments

This work was partly supported by the National Institute of General Medical Sciences (R35GM138264 to K. Tsuchikama), the Department of Defense Breast Cancer Research Program (W81XWH-19-1-0598, to K. Tsuchikama), the Cancer Prevention and Research Institute of Texas (RP150551 and RP190561, to Z. An), the Welch Foundation (AU-0042-20030616, to Z. An), and the Japan Society for the Promotion of Science (postdoctoral fellowship to Y. Anami). We gratefully acknowledge the following researchers for providing the cell lines used in this study: U87ΔEGFR from Prof. Balveen Kaur (UTHealth) and KPL-4 from Dr. Junichi Kurebayashi (Kawasaki Medical School). We thank Prof. Momoko Yoshimoto (UTHealth) for providing a scientific advice on studies using human HSPCs, and Dr. Yoshihiro Otani and Dr. Kyotaro Ohno (Okayama University) for providing a clinical opinion for MRI and liver tissue analysis.

The costs of publication of this article were defrayed in part by the payment of page charges. This article must therefore be hereby marked *advertisement* in accordance with 18 U.S.C. Section 1734 solely to indicate this fact.

Note

Supplementary data for this article are available at Molecular Cancer Therapeutics Online (http://mct.aacrjournals.org/).

Received May 24, 2022; revised June 22, 2022; accepted June 28, 2022; published first July 6, 2022.

References

1. Drago JZ, Modi S, Chandarlapaty S. Unlocking the potential of antibody–drug conjugates for cancer therapy. Nat Rev Clin Oncol 2021;18:327–44.
2. Khongorzul P, Ling CJ, Khan FU, Ihsan AU, Zhang J. Antibody–drug conjugates: a comprehensive review. Mol Cancer Res 2020;18:3–19.
3. Lehar SM, Pillow T, Xu M, Staben L, Kajihara KK, Vandlen R, et al. Novel antibody–antibiotic conjugate eliminates intracellular S. aureus. Nature 2015;527:323–8.
4. Wang RE, Liu T, Wang Y, Cao Y, Du J, Luo X, et al. An immunosuppressive antibody–drug conjugate. J Am Chem Soc 2015;137:3229–32.
5. Esnault C, Schrama D, Houben R, Guyétant S, Desgranges A, Martin C, et al. Antibody-drug conjugates as an emerging therapy in oncodermatology. Cancers 2022;14:778.
6. Bargh JD, Isidro-Llobet A, Parker JS, Spring DR. Cleavable linkers in antibody-drug conjugates. Chem Soc Rev 2019;48:4361–74.
7. Tsuchikama K, An Z. Antibody-drug conjugates: recent advances in conjugation and linker chemistries. Protein Cell 2018;9:33–46.
8. Tang H, Liu Y, Yu Z, Sun M, Lin L, Liu W, et al. The analysis of key factors related to ADCs structural design. Front Pharmacol 2019;10:373.
9. Beck A, Goetsch L, Dumontet C, Corvaïa N. Strategies and challenges for the next generation of antibody–drug conjugates. Nat Rev Drug Discov 2017;16:315–37.
10. Katz J, Janik JE, Younes A. Brentuximab vedotin (SGN-35). Clin Cancer Res 2011;17:6428–36.
11. Deeks ED. Polatuzumab vedotin: first global approval. Drugs 2019;79:1467–75.
12. Chang E, Weinstock C, Zhang L, Charlab R, Dorff SE, Gong Y, et al. FDA approval summary: enfortumab vedotin for locally advanced or metastatic urothelial carcinoma. Clin Cancer Res 2021;27:922–7.
13. Lee A. Loncastuximab tesirine: first approval. Drugs 2021;81:1229–33.
14. Hong DS, Concin N, Vergote I, de Bono JS, Slomovitz BM, Drew Y, et al. Tisotumab vedotin in previously treated recurrent or metastatic cervical cancer. Clin Cancer Res 2020;26:1220–8.
15. Scott LJ. Brentuximab vedotin: a review in CD30-positive Hodgkin lymphoma. Drugs 2017;77:435–45.
16. Younes A, Gopal AK, Smith SE, Ansell SM, Rosenblatt JD, Savage KJ, et al. Results of a pivotal phase II study of brentuximab vedotin for patients with relapsed or refractory Hodgkin's lymphoma. J Clin Oncol 2012;30:2183–9.
17. Nademanee A, Sureda A, Stiff P, Holowiecki J, Abidi M, Hunder N, et al. Safety analysis of brentuximab vedotin from the phase III AETHERA trial in Hodgkin lymphoma in the post-transplant consolidation setting. Biol Blood Marrow Transplant 2018;24:2354–9.
18. Johnson M, El-Khoueiry A, Hafez N, Lakhani N, Mamdani H, Rodon J, et al. Phase I, first-in-human study of the probody therapeutic CX-2029 in adults with advanced solid tumor malignancies. Clin Cancer Res 2021;27:4521–30.
19. Anami Y, Yamazaki CM, Xiong W, Gui X, Zhang N, An Z, et al. Glutamic acid–valine–citrulline linkers ensure stability and efficacy of antibody–drug conjugates in mice. Nat Commun 2018;9:2512.
20. Dorywalska M, Dushin R, Moine L, Farias SE, Zhou D, Navaratnam T, et al. Molecular basis of valine-citrulline-PABC linker instability in site-specific ADCs and its mitigation by linker design. Mol Cancer Ther 2016;15:958–70.
21. Zhao H, Gulesserian S, Malinao MC, Ganesan SK, Song J, Chang MS, et al. A potential mechanism for ADC-induced neutropenia: role of neutrophils in their own demise. Mol Cancer Ther 2017;16:1866–76.
22. Miller JT, Vitro CN, Fang S, Benjamin SR, Tumey LN. Enzyme-agnostic lysosomal screen identifies new legumain-cleavable ADC linkers. Bioconjug Chem 2021;32:842–58.
23. Fu Z, Thorpe M, Akula S, Chahal G, Hellman LT. Extended cleavage specificity of human neutrophil elastase, human proteinase 3, and their distant ortholog clawed frog PR3—three elastases with similar primary but different extended specificities and stability. Front Immunol 2018;9:2387.

24. Anami Y, Tsuchikama K. Transglutaminase-mediated conjugations. Methods Mol Biol 2020;2078:71–82.
25. Anami Y, Xiong W, Gui X, Deng M, Zhang CC, Zhang N, et al. Enzymatic conjugation using branched linkers for constructing homogeneous antibody–drug conjugates with high potency. Org Biomol Chem 2017;15:5635–42.
26. Lyon RP, Bovee TD, Doronina SO, Burke PJ, Hunter JH, Neff-LaFord HD, et al. Reducing hydrophobicity of homogeneous antibody-drug conjugates improves pharmacokinetics and therapeutic index. Nat Biotechnol 2015;33: 733–5.
27. Zhao H, Gulesserian S, Ganesan SK, Ou J, Morrison K, Zeng Z, et al. Inhibition of megakaryocyte differentiation by antibody–drug conjugates (ADCs) is mediated by macropinocytosis: implications for ADC-induced thrombocytopenia. Mol Cancer Ther 2017;16:1877–86.
28. Yardley DA, Krop IE, LoRusso PM, Mayer M, Barnett B, Yoo B, et al. Trastuzumab emtansine (T-DM1) in patients with HER2-positive metastatic breast cancer previously treated with chemotherapy and 2 or more HER2-targeted agents: results from the T-PAS Expanded Access Study. Cancer J 2015; 21:357–64.
29. Poon KA, Flagella K, Beyer J, Tibbitts J, Kaur S, Saad O, et al. Preclinical safety profile of trastuzumab emtansine (T-DM1): mechanism of action of its cytotoxic component retained with improved tolerability. Toxicol Appl Pharmacol 2013; 273:298–313.
30. Yamazaki CM, Yamaguchi A, Anami Y, Xiong W, Otani Y, Lee J, et al. Antibody-drug conjugates with dual payloads for combating breast tumor heterogeneity and drug resistance. Nat Commun 2021;12:3528.
31. Lambert JM, Chari RVJ. Ado-trastuzumab emtansine (T-DM1): an antibody–drug conjugate (ADC) for HER2-positive breast cancer. J Med Chem 2014;57: 6949–64.
32. Okamoto H, Oitate M, Hagihara K, Shiozawa H, Furuta Y, Ogitani Y, et al. Pharmacokinetics of trastuzumab deruxtecan (T-DXd), a novel anti-HER2 antibody-drug conjugate, in HER2-positive tumour-bearing mice. Xenobiotica 2020;50:1242–50.
33. Phillips AC, Boghaert ER, Vaidya KS, Mitten MJ, Norvell S, Falls HD, et al. ABT-414, an antibody–drug conjugate targeting a tumor-selective EGFR epitope. Mol Cancer Ther 2016;15:661–9.
34. Hamblett KJ, Kozlosky CJ, Siu S, Chang WS, Liu H, Foltz IN, et al. AMG 595, an anti-EGFRvIII antibody-drug conjugate, induces potent antitumor activity against EGFRvIII-expressing glioblastoma. Mol Cancer Ther 2015;14: 1614–24.
35. Staben LR, Koenig SG, Lehar SM, Vandlen R, Zhang D, Chuh J, et al. Targeted drug delivery through the traceless release of tertiary and heteroaryl amines from antibody–drug conjugates. Nat Chem 2016;8:1112–9.
36. Doronina SO, Mendelsohn BA, Bovee TD, Cerveny CG, Alley SC, Meyer DL, et al. Enhanced activity of monomethylauristatin F through monoclonal antibody delivery: effects of linker technology on efficacy and toxicity. Bioconjug Chem 2006;17:114–24.
37. Caculitan NG, Chuh JDC, Ma Y, Zhang D, Kozak KR, Liu Y, et al. Cathepsin B is dispensable for cellular processing of cathepsin B-cleavable antibody–drug conjugates. Cancer Res 2017;77:7027–37.
38. Zhang D, Le H, Cruz-Chuh JD, Bobba S, Guo J, Staben L, et al. Immolation of p-aminobenzyl ether linker and payload potency and stability determine the cell-killing activity of antibody–drug conjugates with phenol-containing payloads. Bioconjug Chem 2018;29:267–74.
39. Alley SC, Benjamin DR, Jeffrey SC, Okeley NM, Meyer DL, Sanderson RJ, et al. Contribution of linker stability to the activities of anticancer immunoconjugates. Bioconjug Chem 2008;19:759–65.
40. Doronina SO, Toki BE, Torgov MY, Mendelsohn BA, Cerveny CG, Chace DF, et al. Development of potent monoclonal antibody auristatin conjugates for cancer therapy. Nat Biotechnol 2003;21:778–84.
41. Lyon RP, Setter JR, Bovee TD, Doronina SO, Hunter JH, Anderson ME, et al. Self-hydrolyzing maleimides improve the stability and pharmacological properties of antibody-drug conjugates. Nat Biotechnol 2014;32:1059–62.
42. Zhang S, Zhou D, Zheng C, Xiong P, Zhu W, Zheng D. Preclinical evaluation of a novel antibody-drug conjugate targeting DR5 for lymphoblastic leukemia therapy. Mol Ther Oncolytics 2021;21:329–39.
43. Chuprakov S, Ogunkoya AO, Barfield RM, Bauzon M, Hickle C, Kim YC, et al. Tandem-cleavage linkers improve the in vivo stability and tolerability of antibody-drug conjugates. Bioconjug Chem 2021;32:746–54.
44. Su Z, Xiao D, Xie F, Liu L, Wang Y, Fan S, et al. Antibody-drug conjugates: recent advances in linker chemistry. Acta Pharm Sin B 2021;11:3889–907.
45. Gregson SJ, Barrett AM, Patel NV, Kang G-D, Schiavone D, Sult E, et al. Synthesis and evaluation of pyrrolobenzodiazepine dimer antibody-drug conjugates with dual β-glucuronide and dipeptide triggers. Eur J Med Chem 2019;179:591–607.
46. Peterson JJ, Meares CF. Cathepsin substrates as cleavable peptide linkers in bioconjugates, selected from a fluorescence quench combinatorial library. Bioconjug Chem 1998;9:618–26.
47. Dubowchik GM, Firestone RA, Padilla L, Willner D, Hofstead SJ, Mosure K, et al. Cathepsin B-labile dipeptide linkers for lysosomal release of doxorubicin from internalizing immunoconjugates: model studies of enzymatic drug release and antigen-specific in vitro anticancer activity. Bioconjug Chem 2002;13:855–69.
48. Salomon PL, Reid EE, Archer KE, Harris L, Maloney EK, Wilhelm AJ, et al. Optimizing lysosomal activation of antibody-drug conjugates (ADCs) by incorporation of novel cleavable dipeptide linkers. Mol Pharm 2019;16:4817–25.
49. Yan H, Endo Y, Shen Y, Rotstein D, Dokmanovic M, Mohan N, et al. Ado-trastuzumab emtansine targets hepatocytes via human epidermal growth factor receptor 2 to induce hepatotoxicity. Mol Cancer Ther 2016;15:480–90.
50. Modi S, Park H, Murthy RK, Iwata H, Tamura K, Tsurutani J, et al. Antitumor activity and safety of trastuzumab deruxtecan in patients with HER2-low-expressing advanced breast cancer: results from a phase Ib study. J Clin Oncol 2020;38:1887–96.
51. Wang ES, Baron J. Management of toxicities associated with targeted therapies for acute myeloid leukemia: when to push through and when to stop. Hematology Am Soc Hematol Educ Program 2020;2020:57–66.
52. Mersana Therapeutics, Inc. Mersana Therapeutics announces partial clinical hold for XMT-1522 clinical trial; 2018. Available from: https://ir.mersana.com/news-releases/news-release-details/mersana-therapeutics-announces-partial-clinical-hold-xmt-1522.
53. Pegram MD, Hamilton EP, Tan AR, Storniolo AM, Balic K, Rosenbaum AI, et al. First-in-human, phase 1 dose-escalation study of biparatopic anti-HER2 antibody-drug conjugate MEDI4276 in patients with HER2-positive advanced breast or gastric cancer. Mol Cancer Ther 2021;20:1442–53.
54. Nair AB, Jacob S. A simple practice guide for dose conversion between animals and human. J Basic Clin Pharm 2016;7:27–31.
55. Mahalingaiah PK, Ciurlionis R, Durbin KR, Yeager RL, Philip BK, Bawa B, et al. Potential mechanisms of target-independent uptake and toxicity of antibody-drug conjugates. Pharmacol Ther 2019;200:110–25.